

740. Aeroacoustic testing of the landing gear components

Shuangli Long¹, Hong Nie², Caijun Xue, Xin Xu

State Key Laboratory of Strength and Vibration of Mechanical Structures
Nanjing University of Aeronautics & Astronautics, Nanjing, 210016, China

E-mail: ¹longshuangli@gmail.com, ²hnie@nuaa.edu.cn

(Received 18 November 2011; accepted 14 February 2012)

Abstract. The sound field generated by full scale landing gear components was studied in an acoustic wind tunnel. Noise characteristics were evaluated. The noise contribution of each part was investigated by removing the gear part individually. Three design parameters were also obtained to assess the noise reduction potential. Test results indicate that the noise spectrum of the component is essentially broadband and mainly dominated by some peaks corresponding to the constant St . Sound pressure level scales with the sixth power velocity law. Noise radiation from the components has obvious directivities. The main strut is the least contributor while the bogie is the largest contributor to the total noise. It is also found that the noise level increases with the gear installation angle from 0° to 16.5° while it decreases via changing the torque link layout from the front of the main strut to its back or modifying the bogie shape by filling its holes.

Keywords: wind tunnel, aeroacoustic measurement, aerodynamic noise, landing gear design.

1. Introduction

Landing gear together with high lift devices has been identified as the main source of airframe noise during the approach and landing phase for commercial aircraft [1-4]. The properties, such as the extremely unfriendly aerodynamically shape or the flow interaction with protrusions and cavities, make the landing gear to be one of the least understood aircraft noise contributors [5-6]. The landing gear noise represents a complex aeroacoustic problem and the underlying noise mechanism has been extensively explored.

Wind tunnel experiments are usually conducted to quantify the landing gear noise characteristics. Researchers from the industry and government agencies, such as NASA [7], Boeing [8], DLR [9], Airbus [1], ONERA [10], Messier-Dowty [11], have performed many studies in wind tunnel to identify and reduce landing gear noise on different models and configurations. Guo [12] tested a full-scale Boeing 737 landing gear at Boeing's low speed aeroacoustic facility. It was found that different components had different frequency dependencies on flow parameters and gear geometry. Ravetta [13] tested various configurations of a 26% scale Boeing 777 main landing gear at the Virginia Tech stability wind tunnel. The test gained some insight into the noise generation mechanism for some components. Dobrzynski [14] performed a full-scale test for the Airbus 340 nose and main landing gear. It concluded that the overall noise increased with gear size and number of axles. In more recent work, Zawodny [15] studied a 1/4-scale Gulfstream G550 aircraft nose landing gear. The test obtained an aeroacoustic dataset for nose landing gear during the landing condition.

Several models have been proposed in the past to deal with the landing gear noise prediction [16]. The first empirical model developed by Fink [2] was based on the data from both flight tests and wind tunnel experiments. Then essentially based on the theoretical background, Guo [8, 16] proposed a component-based model which decomposed the landing gear noise into three spectral components. Computational methods [17-19] could be general but such tools have not yet been applied to complex landing gears with details. Results for more generic gear geometries have not been validated.

Many efforts have been made to reduce the landing gear noise. A low-noise gear design [11, 20] has to account for the major constraints. Streamlined add-on fairings to protect complex

gear from high-speed inflow have been tested [5, 9]. In contrast to simple passive means, active control technologies [21] have also been investigated to attenuate the landing gear noise. However, due to the complicated noise generation, few effective methods have been developed to reduce the landing gear noise.

Post landing gear with one wheel is the base of other landing gear configurations and it is primary interest as a prominent noise source. In this paper, the test was conducted in a low speed aeroacoustic wind tunnel at China Aerodynamic Research & Development Center (CARDC), utilizing actual full scale post landing gear components from HO300 aircraft. The test focuses on the noise characteristics, the noise contribution of each gear-part, and noise reduction potential of design parameters. From the test results, the noise characteristics of the noise spectra, the velocity scaling law, and the radiation directivity are studied. The noise contribution of each gear-part is obtained by removing gear-part individually. Three design parameters, i.e. the gear installation angle, the torque link layout and the bogie shape, are chosen to assess noise reduction potential. The results can provide a reference for landing gear noise prediction and low noise landing gear design.

2. Description of Experiment

2.1. Test Model

The model is provided by China Aviation Industry General Aircraft Company. The visualization of the model is shown in Fig. 1. The model features all the gear parts: the main strut, the torque link, the bogie and the wheel. It also includes most details such as tyre thread, holes and bolts. However, the braking device and the retracting system are not included. Any parts located above the cavity plane are omitted, since such parts are the connections to the fuselage in the gear cavity. A six-degree-of-freedom robot arm support system with acoustic absorbent is on the side of the nozzle.

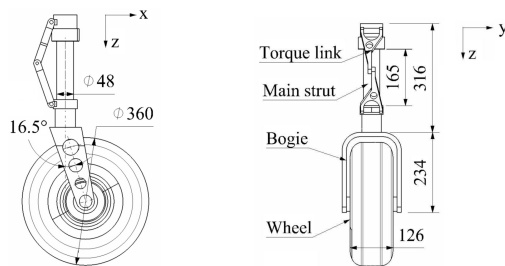


Fig. 1. Visualization of the landing gear model: a) Side view b) Front view (Unit: mm)

2.2. Wind-Tunnel Test Setup

Fig. 2 shows the wind tunnel schematic and a photograph of the test chamber. This facility is designed to provide a low turbulence level flow for dynamic and aeroacoustic measurements. It includes a 400 mm by 550 mm freejet in a large fully anechoic test chamber. The freejet exhaust is through a 940 mm by 810 mm exhaust collector. The chamber with the existing foam wedges allows for broadband measurements, and the lower limiting frequency is 200 Hz. The facility can produce a range of flow speeds. The maximum flow speed can reach up to 100 m/s. In addition, the relatively low turbulent level of this facility is less than 0.05 %.

Fig. 3 shows the Cartesian coordinate system and the location of the microphones in the test. The coordinate origin is defined on the center line of the nozzle and 240 mm from the center point of nozzle. The x -coordinate is defined in the streamwise direction, positive pointing

downstream. The y -coordinate is perpendicular to the ground, positive pointing the ground. The main strut is parallel to the z axis inclining perpendicularly to the flow direction. Three types of microphones were employed in the test. The first was a polar array positioned in plane XOZ . The polar array had two rings of 1500-mm-radius and 2150-mm-radius with respect to the origin. Each ring consisted of 5 microphones (BSWA, 1/2" Prepolarized Condenser Microphone, Type: MP 201) placed at $83^\circ, 98^\circ, 118^\circ, 133^\circ, 148^\circ$ with respect to the X -axis. The microphones in this array were named P1-P10 respectively. The second was a traverse array, which had a 1020-mm-radius ring in plane YOZ . The ring contained five microphones (BSWA, 1/2" Prepolarized Condenser Microphone, Type: MP 201) placed path at $18^\circ, 36^\circ, 54^\circ, 72^\circ, 108^\circ$ with respect to the Y axis. The microphones in this array were named P11-P15 respectively. The last one was a free microphone (B&K, type 2231) located at point (-850mm, 520mm, -60mm). Each microphone was mounted on the test chamber wall. Their surfaces were treated by wind screen to avoid being directly exposed to the wind. The dynamic range of the microphones was set from 30 dB to 140 dB. The polar array and traverse array are used to resolve the directivity of the noise field. The free microphone is used to derive the frequency spectra data.

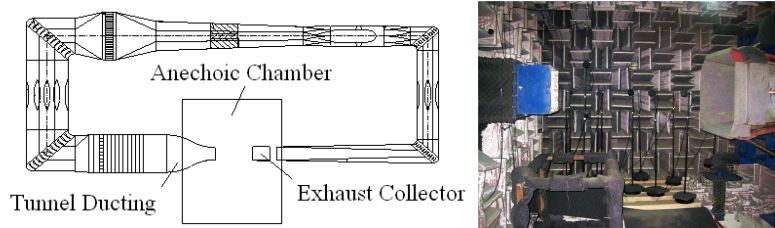


Fig. 2. CARDC's low speed aeroacoustic wind tunnel: a) the tunnel circuit; b) test chamber

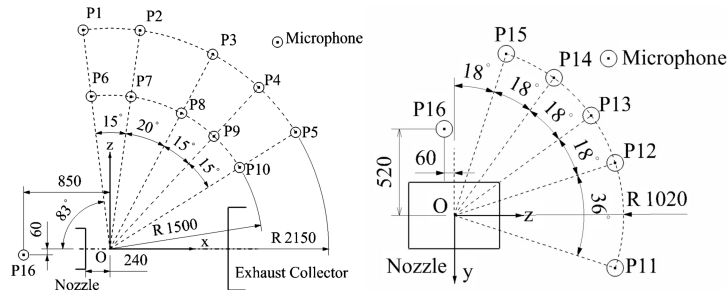


Fig. 3. Measurement equipment locations: a) Polar array; b) Traverse array (Unit: mm)

Each microphone was calibrated by a piston phone (CEL-110/2/RS) before measurement. Noise measurement data was processed by using microphones sensitivities obtained by the calibration. The correction was also made on the basis of the reference sound source (B&K 4204) at each microphone. Considering the microphones were not far from the model, the atmospheric absorption correction was small. So the sound attenuation in the atmosphere was not corrected.

The noise data were acquired three times with a record of 2 s each. Noise spectra are determined by splitting the data into 39 blocks of 2048 samples with an overlap of 50%. Each block is multiplied by a Hanning windowing function before applying a Fast Fourier Transform. The Nyquist frequency of the resulting spectra is 10000 Hz and the frequency resolution is 9.766 Hz. The results of the 117 blocks have been averaged to determine the final spectra. Frequencies below 200 Hz are discarded because of the chamber limit. Considering the relative loudness of sounds in air as perceived by the human ear, A-weighted over frequencies is applied to SPL in spectra [6]. The reference pressure in the data analysis is 20 μ Pa.

2. 3. Test Configurations and Descriptions

It is of great importance to clearly know the source characteristics, to quantify contribution of each part to total noise and to assess design parameters which can lead to lower noise. Since this model is an assembly of individual parts, the task can be possibly conducted.

Firstly, the source characteristics of the baseline configuration A shown in Fig. 4 are investigated. The baseline configuration contains the main strut, the torque link and the bogie. The configuration was tested at flow speeds of 30, 40, 50, 60, 70 and 80 m/s.

Secondly, the contribution from different gear-part is assembly studied by removing gear-part individually. Four configurations with the same side line were tested at flow speeds of 40, 60 and 80 m/s. To facilitate the discussion, all four configurations, shown in Fig. 5, are summarized in Table 1. Operations of these configurations are given in Table 2. The letters in the first column in Table 2 represent the configurations in Table 1.

Finally, three comparisons are made to assess noise reduction potential of the design parameters at flow speeds 40, 60 and 80m/s. Gear installation angle was altered from 0° to 16.5°. The torque link layout was changed from the front of the main strut to its back. The bogie shape was modified by filling its holes.



Fig. 4. Baseline configuration in the test

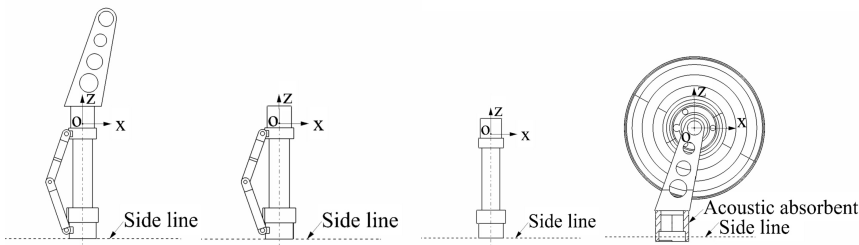


Fig. 5. Schematic of the test configurations: a) A; b) B; c) C; d) D

Table 1. Test configuration and description

Configuration	Description
A	main strut, torque link, bogie
B	main strut, torque link
C	main strut
D	bogie, wheel

Table 2. Noise contribution of the gear-part through configurations operation

Operation	Noise contribution of the part
A-B	Bogie
B-C	torque link
D-(A-B)	Wheel
B+D	Total

Due to the nozzle area limitation, the blockage coefficient is taken into account. The ratio of the configuration A, B, C, D projected area to the nozzle area is about 11%, 8%, 8%, 23%, respectively. In a square open-jet wind tunnel, the magnitude of blockage effect is only about 0.29 of that present in the closed tunnel [22-23]. So the blockage coefficient for configurations A, B, C is acceptable [7]. For configuration D, the error analysis due to the blockage is present. From the equation (1), the velocity increments associated with the solid blockage can be

calculated through the ratio $\Delta V / V$, which is ε_s in the (1). For the all the velocity tested about configuration D, the velocity error $\Delta V / V$ is about 2%.

$$\varepsilon_s = -0.211 \frac{Vol}{\beta^3 h^3} \quad (1)$$

Vol is the model volume, β is $(1-M^2)^{1/2}$, M is Mach number, h is the height of the tunnel.

3. Results and Discussion

3. 1. Source Characteristics

Fig. 6 shows normalized A-weighted narrow band spectra for baseline configuration and background noise at P16. The SPL have been normalized by a constant propagation distance r_{ref} based on spherical sound attenuation relative to the measurement distance r . In this paper, $r_{ref} = 1 \text{ m}$ is chosen. It can be observed that the differences between baseline and background noise are all greater than 10 dB. So the noise source could be identified effectively by the microphone. The SPL is continuously increased with the flow speed. The spectra are essentially broadband and mainly dominated by some peaks.

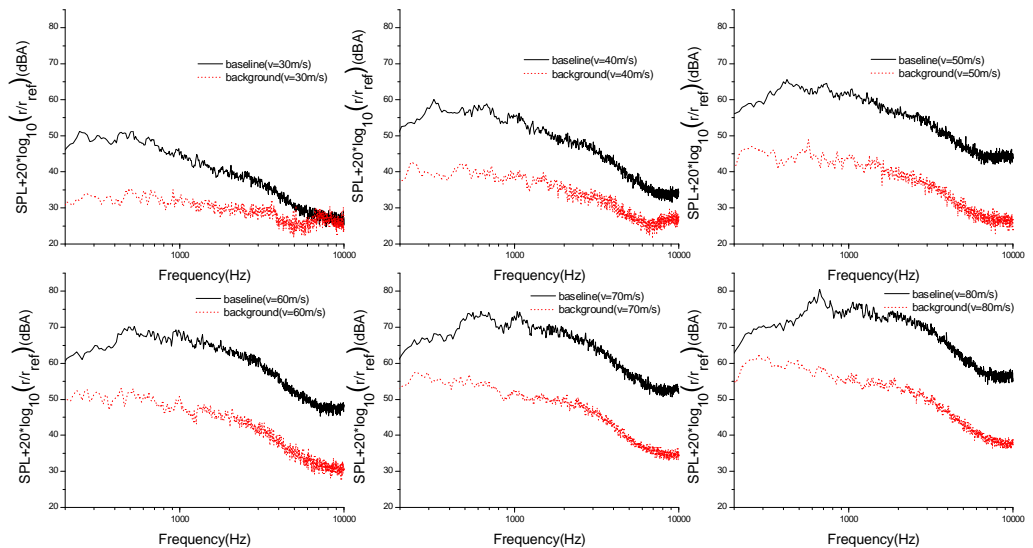


Fig. 6. Normalized A-weighted spectra for baseline configuration and background at P16

Fig. 7 is A-weighted 1/3-oct band spectra versus St ($St = fD / V$, where f is frequency, D is the characteristic length, and V is flow speed) for baseline configuration at different flow speeds at P16. In this paper, a value of $D = 360 \text{ mm}$ corresponding to wheel diameter is chosen. The reference speed is $V_{ref} = 100 \text{ m/s}$. It shows that the data fit the sixth power scaling well when St is less than 19. It indicates that the source is dipoles furnished by the unsteady forces on the body surfaces. When St is above 19, radiation degrades from the dipoles to quadrupole because the noise reflects and diffracts from the unsteady flow, which scales on the eighth power law. Fig. 7 also illustrates that peaks in the spectra scale on $St \approx 2.8$, $St \approx 5.7$, $St \approx 9$ at different flow speed.

Fig. 8a) is the noise at polar array microphone P1-P10 in the plane XOZ radiated from the baseline configuration. The results show that in polar radiation directivity is from 83° to 148° . Noise radiates predominantly in backward arc, peaking at 148° , and the minimum value is at 83° . Fig. 8b) is the noise at the traverse array microphone P11-P15 in the plane YOZ radiated from the baseline configuration. The results indicate that in the traverse angle from 18° to 108° , noise radiates predominantly in the lateral arc, peaking at 18° and the minimum value is at 90° . The OASPL on P11 is almost equal to the value on P12. It is noticed that the two points and the configuration are approximate symmetry about the axis z , so the directivity could also symmetry about the axis z .

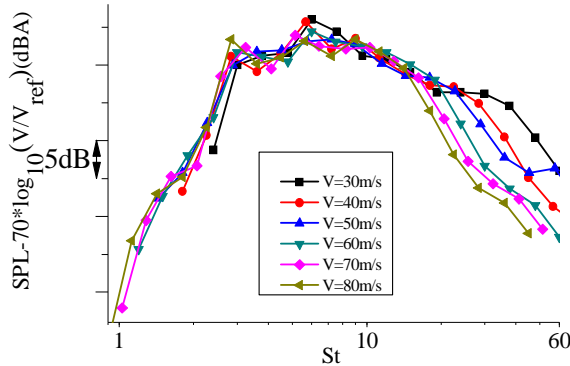


Fig. 7. Non-dimensional A-weighted 1/3 octave band by sixth power scaling law

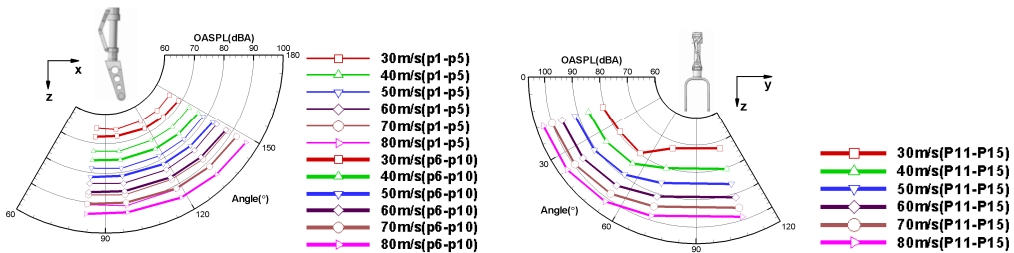


Fig. 8. Directivity of baseline configuration from the arrays a) Polar array b) Traverse array

3. 2. Noise Contribution from Different Gear-part

The narrow band SPL comparison of configuration B, C, D with the wind tunnel background noise at different flow speed on P16 can be observed in Fig. 9. The results suggest that the signal to noise ratio of this measurement is actually comfortable at all wind velocities and in the whole frequency band.

The effect of the bogie is shown in Fig. 10a), which plots the normalized A-weighted 1/3 octave band spectra of configuration A and B at different flow speeds on P16. There is noticeable difference for frequencies between the spectra. The St difference is between 1.8 and 9, where the SPL difference is between 6-4 dB at all flow speeds. When the St is below 1.8, the spectra of the two configurations fit well; when St is above 9, there is about 1 dB SPL difference. The results indicate that the bogie noise is mainly between $St = 1.8$ and $St = 9$. Adding the bogie to configuration B also brings some new detail features and produces some vortex corresponding to the high frequency noise. Thus there is little different in SPL when St is below 1.8, however, there is about 1 dB in SPL when St was above 9. Two peaks are found at $St = 2.8$ and $St = 5.7$ from the spectra of configuration A. However, no apparent peak could be found at these St from the spectra of the configuration B. The results indicate these peaks are relevant to

the bogie noise.

The effect of the main strut can be observed in Fig. 10b), which is the normalized A-weighted 1/3 octave band spectra of configuration C at different flow speeds on P16. The frequencies of the first peak in the spectra are dominating frequencies of the main strut. The dominating frequencies have the same $St = 1.5$ corresponding to the characteristic length $D = 360\text{mm}$ which is the wheel diameter. If the characteristic length D changed to the main strut diameter $D = 48\text{mm}$, the St is equal to 0.2. This fits the results of the previous experiment on flow around the cylinder [24]. It indicates the main strut noise is generated by flow separation off the cylinder.

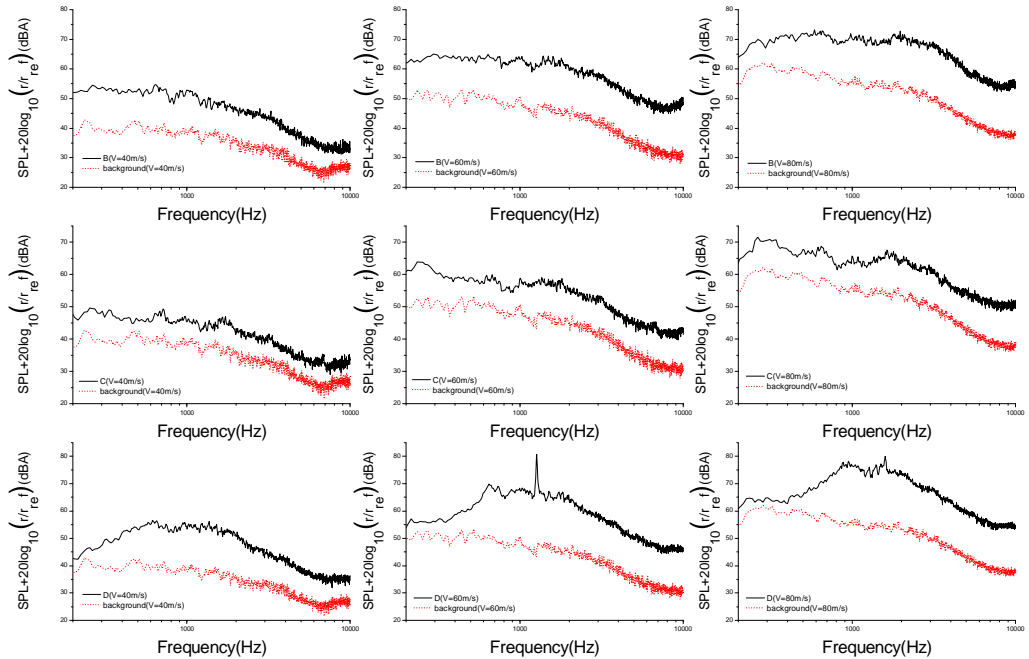


Fig. 9. Normalized A-weighted spectra for configuration B, C, D and background noise at P16

The effect of the torque link is also shown in Fig. 10b). The SPL have an almost uniform increase 4-6 dB when St is above 1.5. This clearly demonstrates the torque link is a very important contributor to the total noise. In the spectra of B, there are three peak frequencies corresponding to $St = 2.9, 5.7,$ and $9,$ respectively. The SPL value at $St = 9$ is the maximum in the three peaks. Considering the torque link is in front of the main strut, there may be interaction noise between the two configurations.

Wheel contribution can be derived through taking the operation: D minus the bogie contribution. Considering the relative location of the wheel and the bogie forms a cavity; there may be interaction noise between the two configurations. So the wheel contribution here contains purely wheel noise and the interaction noise between the wheel and bogie.

Fig. 11 shows the operation results at different flow speeds on P16. The normalized A-weight OASPL is 79.16 dB, 92.21 dB and 100.12 dB corresponding to the flow speed 40, 60, 80 m/s, respectively. The main strut is the least contributor and the bogie is the largest contributor to the total noise. During the operation, the torque link noise is included the interaction noise between the torque link and main strut. The wheel noise includes the interaction noise between the wheel and bogie. So the contribution of them varies with the flow speed.

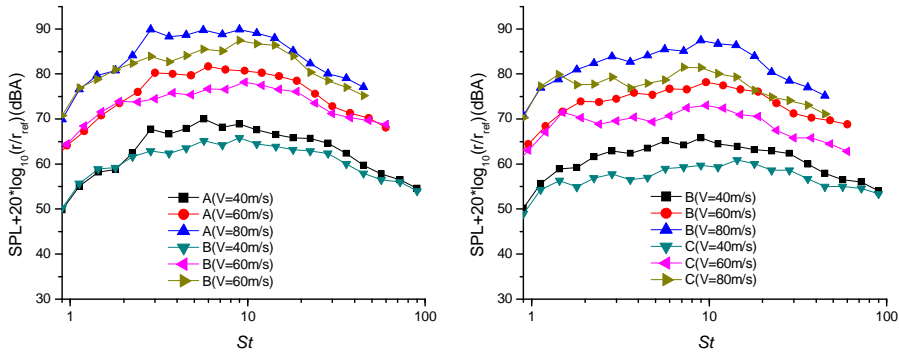


Fig. 10. Normalized A-weighted 1/3 octave band spectra at different flow speeds on P16: SPL versus St
a) Effect of the bogie b) Effect of the main strut and torque link

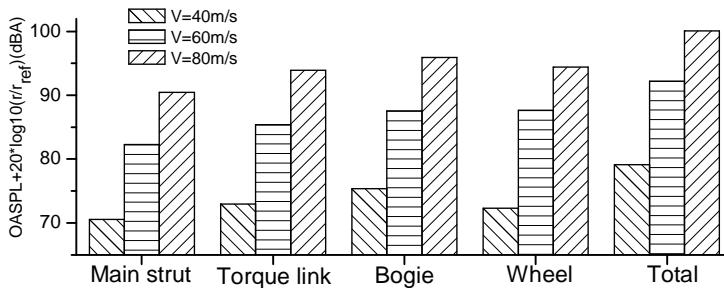


Fig. 11. Contribution of each component to total noise at different flow speeds on P16

3. 3. Noise Reduction Potential of the design parameters

A changed configuration (let us name it A') was made on the basis of configuration A. The installation angle is altered from 0° to 16.5° . The effect of installation angle is shown in Fig. 12a), which plots the normalized A-weighted 1/3 octave band spectra at different flow speeds on P16. It should be noted that the difference is significant for St between 3 and 7, where the SPL of the configuration A' is 4-6dB more than that of the configuration A. When the St is below 3, the spectra of the two configurations fit well. When the St is above 7, there is about 1 dB attenuation. It indicates that increasing the installation angle does not change noise spectra in the low-frequency but it can reduce a little noise mainly in the high frequencies.

The torque link was moved from front of the main strut to its back. The altered configuration (let us name it B') was based on configuration B. The effect of the torque link layout is shown in Fig. 12b), which plots the normalized A-weighted 1/3 octave band spectra at different flow speeds on P16. It can be observed that the difference is significant for St above 2.9, where the SPL of configuration B' is 3-6 dB less than that of the configuration B. When the St is below 2.9, the spectra of the two configurations fit well. The results indicates that the changes can attenuate the SPL from $St = 2.9$. There is not much effect on the spectra when St is below 2.9.

Mechanism of the torque link noise can be analyzed from the spectra comparison in Fig. 12b). In the spectra of configuration B, there are three peaks when $St = 2.9, 5.7,$ and $9,$ respectively. However, in the spectra of B', there is only one peak when $St = 2.9$. The two configurations have the first peak at the same St . The noise of both configurations contained the flow noise and interactive noise. The flow noise is decided by the bluff body geometry while interaction noise is decided by the position of the bluff body. Thus, the noise, which is the same part in the spectra of the two configurations, could be flow noise produced by flow separation

off the main strut and the torque link. As it has been mentioned above, the dominant St of the main strut is 1.5 corresponding to the characteristic length of the wheel diameter. Hence it could be deduced that the peak $St = 2.9$ is produced by flow separation off the torque link. The noise, which is the different part of the spectra, is determined by the interaction effect of the torque link and main strut. The results indicate that the different peaks in the spectra between the two configurations are caused by the interaction noise.

Using the vacuum plastic mud to fill the holes on the bogie was done based on the configuration D. Let us name this configuration D'. The effect of modifying the bogie shape is shown in Fig. 12c) and 12d), which plots the normalized A-weighted narrow band spectra and 1/3 octave band spectra at different flow speeds on P16. It can be observed that there is a tone appearing in the spectra of the configuration D. The frequencies of the tone increase with the flow speed. The peak level of the tone firstly increases rapidly with the flow speed up to 60 m/s then decreases rapidly with the flow speed. The max peak occurs at 60 m/s. That is to say, the peak level lessens no matter whether the flow speed increases or decreases from 60 m/s. It indicates that particular flow speeds can excite the tone noise, which is a kind of resonance caused by the interactive between the bogie and wheel. The tone noise is eliminated by filling the holes on the bogie. It also can be clearly seen that the difference is significant for St between 2.9 and 9 where the SPL of the configuration D' is 3-6 dB less than that of configuration D. The results indicate that the modification of the bogie shape by filing the holes have important effect on attenuating the bogie noise and eliminating the tone noise.

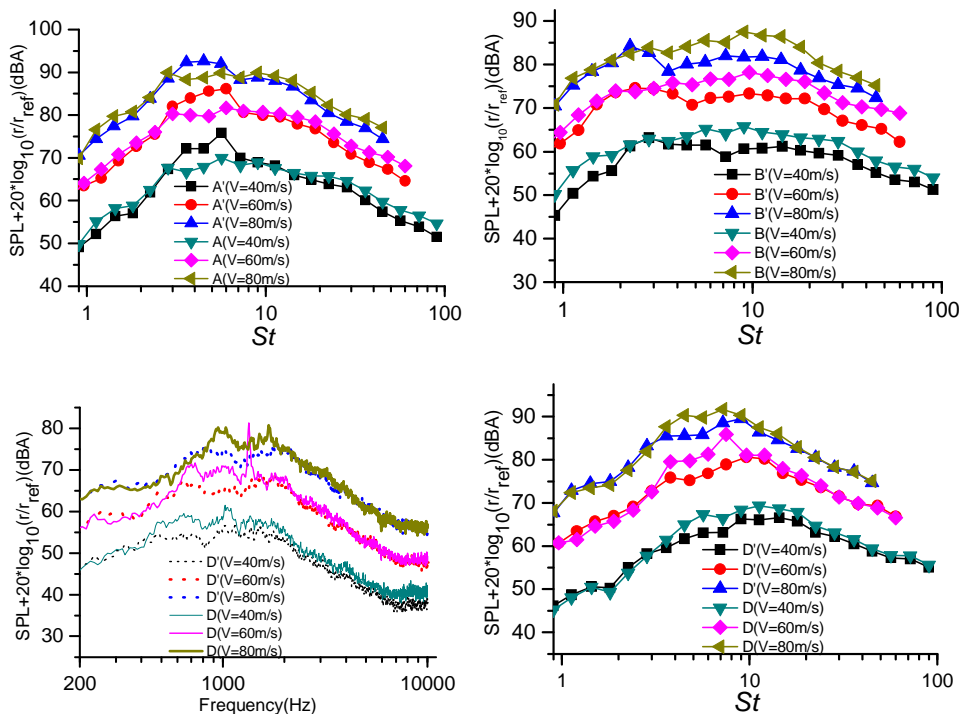


Fig. 12. Normalized A-weighted spectra at different flow speeds on P16: a) effect of altering gear install angle (1/3 octave band); b) effect of changing the torque link layout (1/3 octave band); c) effect of modifying the bogie shape (narrow band); d) the effect of modifying the bogie shape (1/3 octave band)

The methods discussed above indicate that altering the installation angle increases the noise level. Changing the torque link layout and modifying the bogie shape reduce the noise level. These noise reduction potential of the design parameters at different flow speeds are shown in

Fig. 13, which reveals that altering the torque link layout nearly results in about 0.8 dB reduction for all the flow speeds. Modifying bogie shape can lead to about 0.4 dB attenuations at 40 m/s and 80 m/s, while it can lead to 1 dB attenuations at 60 m/s. This is because the tone noise excited at 60 m/s is eliminated. Taking both noise reduction methods, the reduction is about 1.2 dB, compared to the total noise radiated by previous one at all flow speeds.

4. Conclusions

Noise characteristics of landing gear components are investigated in the open jet low speed aeroacoustic wind tunnel. By testing a series of gear configurations, contributions of independent gear part to the total noise are obtained. The noise reduction potential of three design parameters is assessed. The following conclusions are drawn. The landing gear components spectra are essentially broadband and mainly dominated by some peaks corresponding to the constant St . Sound pressure level scales with the sixth power of velocity. The polar radiation of components is predominantly in backward arc while the traverse radiation is predominantly in the lateral arc. The main strut is the least contributor and the bogie is the largest contributor to the total noise. Altering the installation angle of the landing gear from 0° to 16.5° increases the noise. Changing the torque link layout from front of the main strut to its back reduces the noise. Modifying bogie shape by filling its holes attenuates bogie noise including the tone noise as well.

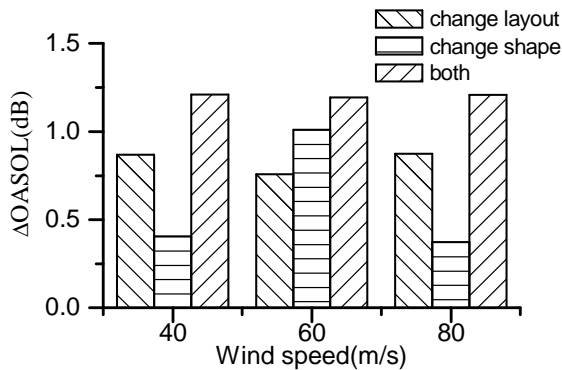


Fig. 13. Noise reduction potential of design parameters at different flow speed on P16

Acknowledgments

The authors would like to acknowledge the China Aerodynamic Research & Development Center for providing the Low Speed Aeroacoustic Facility and China Aviation Industry General Aircraft Company for providing the landing gear model used in this test. We also wish to thank Qiang Zhang, Bo Qin, Yuan Xu from Nanjing University of Aeronautics and Astronautics for their assistance during the wind tunnel experiments. Their support is greatly appreciated.

The financial support from the innovative project for postgraduate cultivation of Jiang Su Province (CX10B_105Z, CX10B_088Z) and China Aviation Science Fund (2009ZA52001) is greatly appreciated. The financial support from China Scholarship Council is also gratefully acknowledged.

References

- [1] Dobrzynski W. Almost 40 years of airframe noise research: what did we achieve? Journal of Aircraft, 2010, Vol. 47, Issue 2, 2010, p. 353-367.

- [2] **Fink M. R.** Noise component method for airframe noise. *Journal of Aircraft*, Vol. 16, Issue 10, 1979, p. 659-665.
- [3] **Elkoby R., Brusniak L., Stoker R. W.** Airframe noise results from the QTD II flight test program. 13th AIAA/CEAS Aeroacoustics Conference (28th AIAA Aeroacoustics Conference), Rome, Italy, 2007, AIAA 2007-3457.
- [4] **Soderman P. T.** Airframe noise study of a Bombardier CRJ-700 aircraft model in the NASA Ames 7- by 10-foot wind tunnel. *Journal of Aeroacoustics*, Vol. 3, Issue 1, 2004, p. 1-42.
- [5] **Boorsma K., Zhang X., Molin N.** Landing gear noise control using perforated fairings. *Acta Mech. Sin.*, Vol. 26, Issue 1, 2010, p. 159-174.
- [6] **Smith M., Carrilho J., Molin N.** Modelling landing gear noise with installation effects. 13th AIAA/CEAS Aeroacoustics Conference (28th AIAA Aeroacoustics Conference), Rome, Italy, 2007, AIAA 2007-3472.
- [7] **Lazos B. S.** Mean flow features around the inline wheels of four-wheel landing gear. *AIAA Journal*, Vol. 40, Issue 2, 2002, p. 193-198.
- [8] **Guo Y. P.** A statistical model for landing gear noise prediction. *Journal of Sound and Vibration*, Vol. 282, 2005, p. 61-87.
- [9] **Dobrzynski W., Ewert R., Pott-Pollenske M.** Research at DLR towards airframe noise prediction and reduction. *Aerospace Science and Technology*, Vol. 12, 2008, p. 80-90.
- [10] **Blacodon D.** Analysis of the airframe noise of an A320/A321 with a parametric method. *Journal of Aircraft*, Vol. 44, Issue 1, 2007, p. 26-34.
- [11] **Dobrzynski W., Chow L. C., Smith M.** Experimental assessment of low noise landing gear component design. *International Journal of Aeroacoustics*, Vol. 9, Issue 6, 2010, p. 763-786.
- [12] **Guo Y. P., Yamamoto K. J.** Experimental study on aircraft landing gear noise. *Journal of Aircraft*, Vol. 43, Issue 2, 2006, p. 306-317.
- [13] **Ravetta P. A., Burdisso R. A., Ng W. F.** Wind tunnel aeroacoustic measurement of a 26%-scale 777 main landing gear model. 10th AIAA/CEAS Aeroacoustics Conference, Manchester, UK, 2004, AIAA 2004-2885.
- [14] **Dobrzynski W., Chow L. C., Cuion P.** An European study on landing gear airframe noise sources. 6th AIAA/CEAS Aeroacoustics Conference and Exhibit, Lahaina/Hawaii, USA, 2000, AIAA 2000-1971.
- [15] **Zawodny N. S., Liu F., Yardibi T.** A comparative study of a 1/4 scale Gulfstream G550 aircraft nose gear model, 15th AIAA/CEAS Aeroacoustics Conference (30th AIAA Aeroacoustics Conference), Miami, USA, 2009, AIAA 2009-3153.
- [16] **Guo Y. P.** A semi-empirical model for aircraft landing gear noise prediction. 12th AIAA/CEAS Aeroacoustics Conference (27th AIAA Aeroacoustics Conference), Cambridge, UK, 2006, AIAA 2006-2627.
- [17] **Lockard D. P., Khorramim M. R., Li F.** Aeroacoustic analysis of a simplified landing gear. 9th AIAA/CEAS Aeroacoustics Conference and Exhibit, South Carolina, USA, 2003, AIAA 2003-3111.
- [18] **Souliez F. J., Long L. N., Morris P. J.** Landing gear aerodynamic noise prediction using unstructured grids. *International Journal of Aeroacoustics*, Vol. 1, Issue 2, 2002, p. 115-135.
- [19] **Sanders L., Manoha E., Khelil S. B.** LAGOON: CFD/CAA coupling for landing gear noise and comparison with experimental database. 17th AIAA/CEAS Aeroacoustic Conference (32nd AIAA Aeroacoustics Conference), Portland, USA, 2011, AIAA-2011-2822.
- [20] **Dobrzynski W., Schöning B., Chow L. C.** Design and testing of low noise landing gears. 11th AIAA/CEAS Aeroacoustics Conference (26th AIAA Aeroacoustics Conference), Monterey, USA, 2005, AIAA 2005-3008.
- [21] **Huang X., Zhang X., Li Y.** Broadband flow-induced sound control using plasma actuators. *Journal of Sound and Vibration*, Vol. 329, 2010, p. 2477-2489.
- [22] **Jewel B. B., William H. R., Alan P.** Low-speed wind tunnel testing. New York: John Wiley & Sons Institute, 1999.
- [23] **Garner H. C., Rogers E. W. E., Acum W. E. A.** Subsonic wind tunnel wall corrections. Teddington: National Physical Laboratory, 1966.
- [24] **Long S. L., Nie H., Xu X.** Numerical simulation of noise induced by flow around a cylinder at different Reynolds number. *Technical Acoustics*, Vol. 30, Issue 2, 2011, p. 111-116.